

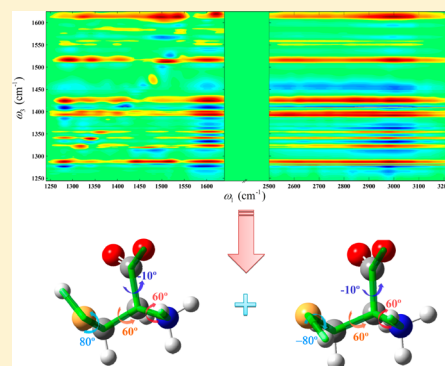
Molecular Conformations of Crystalline L-Cysteine Determined with Vibrational Cross Angle Measurements

Hailong Chen, Hongtao Bian, Jiebo Li, Xunmin Guo, Xiewen Wen, and Junrong Zheng*

Department of Chemistry, Rice University, Houston, Texas 77005, United States

S Supporting Information

ABSTRACT: The molecular conformations of crystalline L-cysteine prepared in its orthorhombic form were determined by the vibrational cross angle measurements. Its major dihedral angles of chemical bonds determined by this method are consistent with the results from diffraction experiments. In addition, the relative orientations of the chemical bonds associated with the hydrogen atoms of the NH_3^+ group and the thiol group are also determined. The results demonstrate that the vibrational cross angle method based on the multiple-mode approach can potentially become a structural tool for determining molecular conformations. The major challenges for the method to become a general molecular structural tool are discussed, and some approaches to address them are proposed.



1. INTRODUCTION

Conformational fluctuations of molecules play critical roles in many chemical and biological processes, such as catalysis, cell signaling, and the fusion of biological membranes.^{1–3} In liquids, conformations of many peptides or proteins can be determined with NMR, and in single crystals X-ray diffraction (XRD) is the best tool for this purpose.^{4–11} So far, these two methods have been proved to be the most powerful nondestructive molecular structural tools. Similar to many other things, at the current stage, these two methods also have some limitations that impose difficulties for them to measure many molecular phenomena, e.g., some special requirements of the sample states, the small XRD cross section of H atom, and the sensitivity to the molecular magnetic properties.^{12,13}

The ultrafast multiple-dimensional vibrational spectroscopy, viewed as an optical analogue of multidimensional nuclear magnetic resonance by many people,^{14,15} have been demonstrated to be able to provide some molecular information that is difficult to be obtained from those traditional methods.^{16–26} In principle, many intrinsic properties of the ultrafast nonlinear vibrational spectroscopy place it in a unique position to be potentially able to resolve molecular structures in many situations that current NMR or XRD techniques can have difficulties to deal with. For instances, its ultrafast temporal resolution (~ 100 fs) enables it to take “snapshots” of fast nuclear motions involved in many molecular conformational changes. The relative ease of manipulating the IR pulses allows the samples to be in almost any condensed phases, e.g., liquids, crystals, amorphous powder, gel, nanoparticles, or interfaces. The method is also immune to the problem of small cross sections of H atoms in XRD or the issue of molecular magnetic properties in NMR measurements. The relatively small amount of sample (ca. $>10^{-8}$ gram, estimated from the sample volume

within the laser focus spot) required for a measurement is also an advantage (over NMR). Inspired by the seemingly promising advantages of the method, in the past few years, we have been focused on developing a special version of ultrafast nonlinear vibrational spectroscopic technique into a molecular structural tool for determining molecular conformations with vibrational cross angle measurements, molecular distances with vibrational energy transfer measurements, and relative intermolecular orientations with molecular heat transport measurements,^{26–35} seeking to understand the opportunity and limitation of the method in resolving molecular structures and conformations in condensed phases. The technique we developed utilizes the synchronization of a picosecond (ps, 10^{-12} second) OPA (Optical Parametric Amplifier) pumped by a ps amplifier and a femtosecond (fs, 10^{-15} second) OPA pumped by a fs amplifier to provide sufficiently high excitation power and a very wide frequency tunability. Recently, we introduced a revised version of the technique with an ultrafast IR/THz super continuum pulse to replace the regular ultrafast IR pulse from the fs OPA as the detection beam.^{27,33} Such a revision simplifies the operation of the lasers. Because of the improvement, the determination of molecular conformations of relatively complex molecules becomes much more practical.²⁷

In previous works, we demonstrated that the conformations of molecules with one or two internal rotational degrees of freedom can be determined with the technique by measuring

Special Issue: Michael D. Fayer Festschrift

Received: June 24, 2013

Revised: August 26, 2013

Published: August 27, 2013

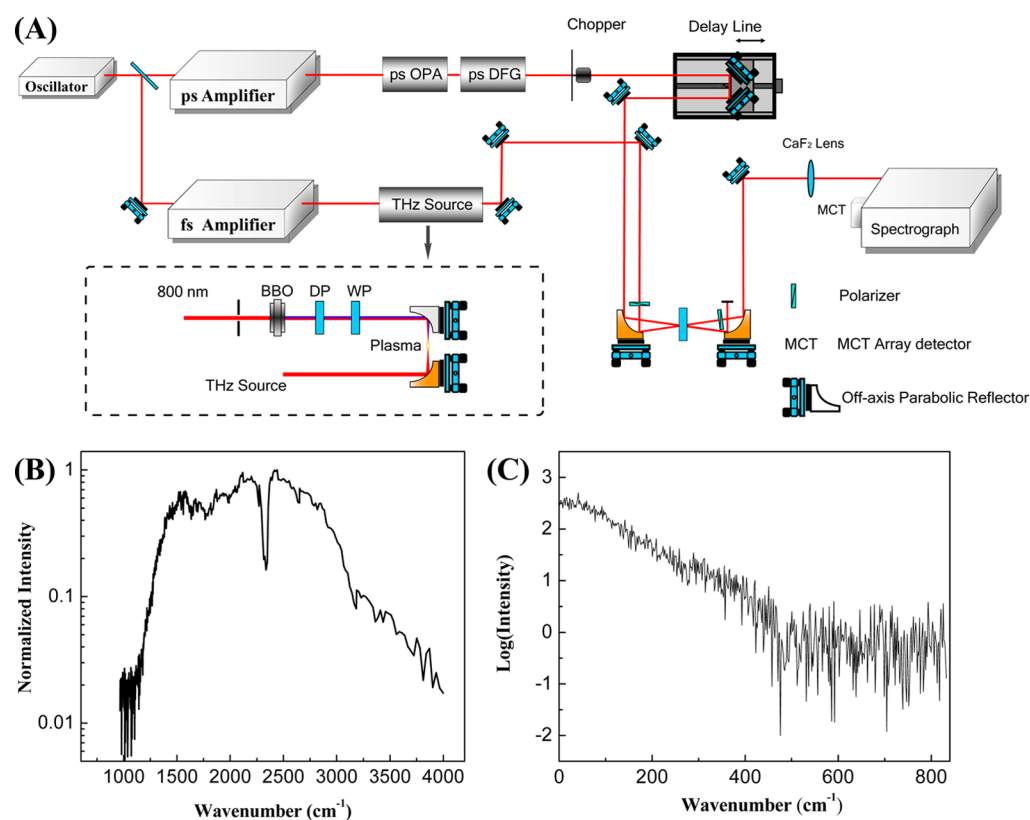


Figure 1. (A) Laser setup. The Mid-IR excitation pulse is generated from the ps OPA and ps DFG setup pumped by the ps amplifier. The mid-IR and terahertz supercontinuum pulse is generated from the optical setup shown in the dashed box, used as the ultrabroadband-probe pulse. (B) Spectrum of the supercontinuum pulse in the high frequency range measured with a liquid-nitrogen-cooled mercury–cadmium-telluride (MCT) array detector. The low-frequency cutoff is caused by the low efficiencies of the grating and the MCT detector. (C) Spectrum of the supercontinuum in the low frequency range measured with the air-breakdown-coherent-detection (ABCD) method.

the relative orientations of the transition dipole moments of different vibrational modes in liquids, solids and on the surfaces of nanoparticles.^{32–34} However, the conformation-mapping strategy that calculates all possible conformations rotating about all single bonds of the molecule introduced in the works is not practical for molecules with more internal rotational degrees of freedom, because there can be too many conformations required to be calculated for a big molecule. For example, if a molecule has four major single bonds, the number of its possible conformations rotating about these bonds for every 10° is $36^4 = 1679616$. In this work, we use a crystalline amino acid, *L*-cysteine, which has four major single bonds about which the rotation can generate many possible molecular conformations, as a model system to explore the possibility to avoid such a straightforward and thorough but extremely time-consuming mapping strategy by combining prior molecular knowledge into consideration to reduce the calculation load. There are two more motivations to choose *L*-cysteine as the model system. One is that the conformations of *L*-cysteine have been well characterized by the diffraction methods,^{36–38} which can be used to benchmark the method. The other is to accumulate a database of nonlinear vibrational properties of amino acids prepared for resolving structures and conformations of peptides or even proteins in the future.

2. EXPERIMENTS AND METHODS

Most of the data presented in the work were collected from a setup described previously.³⁰ Some of the data were obtained from the new IR/IR-T-Hz setup illustrated in Figure 1A.

Briefly, a ps amplifier and a fs amplifier are synchronized with the same seed pulse. The ps amplifier pumps an OPA to produce ~ 0.8 ps (varying from 0.7–0.9 ps in different frequencies) mid-IR pulses with a bandwidth of 10–35 cm⁻¹ in a tunable frequency range from 400 cm⁻¹ to 4000 cm⁻¹ with energy of 1–40 μ J/pulse (1–10 μ J/pulse for 400 cm⁻¹ to 900 cm⁻¹ and >10 μ J/pulse for higher frequencies) at 1 kHz. Light from the fs amplifier is used to generate a high-intensity mid-IR and terahertz supercontinuum pulse by producing plasma in air.^{33,39–41} The collimated 800 nm beam from the fs amplifier is frequency-doubled by passing through a Type-I 150- μ m-thick BBO crystal cut at 29.2° to generate the 400 nm light. A dual wave plate is used to tune the relative polarizations of the 800 and 400 nm pulses operating as a full-wave plate at 400 nm and a half-wave plate at 800 nm. Temporal walkoff between two beams is compensated by inserting a 2-mm-thick BBO (cut at 55°) between the doubling crystal and the wave plate, where the 800 and 400 nm pulses propagate at orthogonal polarizations at different velocities in the delay plate. The supercontinuum pulse is generated by focusing the two copropagating beams on air, with a pulse duration around 110 fs in the frequency range from <20 cm⁻¹ to >3500 cm⁻¹ at 1 kHz (see Figure 1B,C), and the shot to shot fluctuation for every 1000 shots is less than 1% in most of the spectral region (>1000 cm⁻¹. The stability below 1000 cm⁻¹ has not been measured).

In the nonlinear IR experiments, the ps IR pulse is the excitation beam (the excitation power is adjusted based on need and the interaction spot varies from 100 to 500 μ m). The

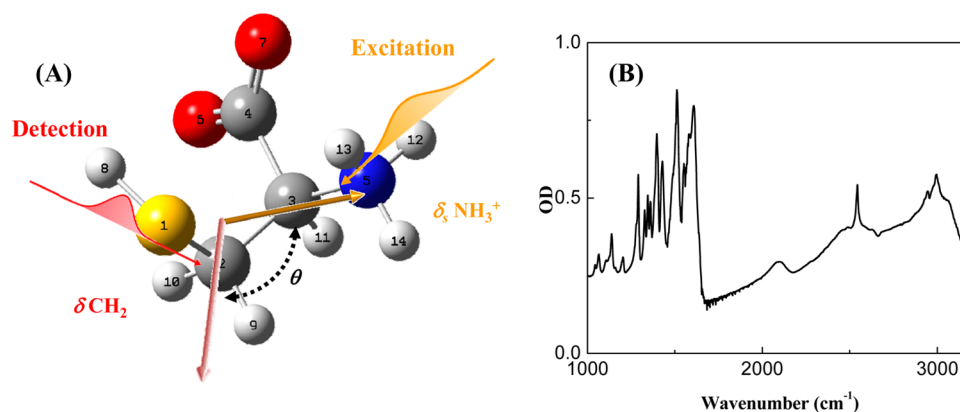


Figure 2. (A) The typical molecular conformation of L-cysteine in its zwitterionic form and the illustration of how the vibrational cross angle between two modes is experimentally determined. (B) FTIR spectrum of the L-cysteine sample. The major peaks involved in the cross angle measurements: NH_3 asymmetrical bending ($\delta_a \text{NH}_3^+$, 1608 cm^{-1}), NH_3 symmetrical bending ($\delta_s \text{NH}_3^+$, 1511 cm^{-1}), CH_2 bending (δCH_2 , 1424 cm^{-1}), CC stretching and CH bending (νCC and δCH , 1396 cm^{-1}), CH bending (δCH , 1343 cm^{-1}) and CH bending and CO_2 symmetrical stretching (δCH and $\nu_s \text{COO}^-$, 1290 cm^{-1}).

supercontinuum pulse is the detection beam frequency-resolved by a spectrograph (resolution is 1–3 cm^{-1} dependent on the frequency) yielding the detection axis of a 2D IR spectrum. Scanning the excitation frequency yields the other axis of the spectrum. Two polarizers are added into the detection beam path immediately behind the sample to selectively measure the parallel or perpendicular polarized signal relative to the excitation beam. Vibrational lifetimes are obtained from $I_{\text{life}} = I_{\parallel} + 2 \times I_{\perp}$, where I_{\parallel} , I_{\perp} are parallel and perpendicular data respectively, and the time dependent anisotropy is obtained from $R = (I_{\parallel} - I_{\perp}) / (I_{\parallel} + 2 \times I_{\perp})$. The setup including the frequency tuning and polarization selection is computer controlled. One of the advantages of the setup over the broad-band pump/probe or 2D IR techniques, besides that it has extreme high excitation power and very broad frequency tunability is that, in the cross peak or 1–2 transition peak measurements, the frequencies contained in the pump pulse do not overlap with those of the frequency-resolved signals. Therefore, the scattered light from the pump pulse does not affect the 2D IR and pump/probe signals obtained from this technique.

L-Cysteine was purchased from Aldrich, and the crystalline sample was prepared by evaporating its aqueous solution on CaF_2 window surface. The isotropic orientation of molecules within the laser focus spot was verified by measuring the samples with different orientations relative to the optical table. The XRD data of the sample is provided in the Supporting Information, which indicates that the orthorhombic form of L-cysteine (L-cysteine-I) is mostly populated in the sample. All measurements were carried out at room temperature (21 $^{\circ}\text{C}$).

DFT calculations were used to convert atomic coordinates (relative atomic orientations) into vibrational coordinates (relative vibrational orientations). In this work, the DFT calculations were carried out using Gaussian 09. The level and basis set used was Becke's 3-parameter hybrid functional combined with the Lee–Yang–Parr correction functional, abbreviated as B3LYP, and 6-311++G(d,p). The vibrational transition moment directions of L-cysteine were calculated with a high dielectric constant (of water) by using SCRF-CPCM to maintain its zwitterion structure. The transition dipole directions of a vibrational mode at the H-bonded state and the free state are typically different because the direction is that of the eigenvector of the sum result of intermolecular

interactions. However, the experimental cross peak intensity is mainly from the local vibrational coupling. In other words, intramolecular couplings dominate over intermolecular interactions. As measured in our previous work, the cross peak intensity from the intramolecular coupling between a combination band and the CN stretch of SCN^- is much stronger than that of the cross peak between the OD stretch and the CN stretch of SCN^- in a $\text{KSCN}/\text{D}_2\text{O}$ solution where SCN^- is believed to form a H-bond with D_2O .^{33,42} Therefore, using the calculated delocalized transition dipole directions from a H-bonded (or intermolecularly interacted) species to analyze the experimental results will cause a big error, as we have tested for the previous systems.^{27,32} To solve this problem, we have developed a procedure for the calculations:^{27,32} (1) to optimize the structure of a H-bonded molecule with a H-bonded partner, and (2) to calculate the vibrational transition dipole directions of this molecule with the H-bonded structure but without the H-bonded partner. In the calculations, the molecular structure is H-bonded, but the transition dipole directions are localized intramolecularly because the H-bonded partner is not involved in the transition dipole calculations. In the previous systems,^{27,32} we found that results through this procedure are not very different from those by directly calculating the isolated nonbonded molecule, probably because intermolecular interactions do not change the molecular structure (in terms of bond lengths) significantly. In addition, as demonstrated, the calculated transition dipole directions of relatively localized modes with different calculation levels are very similar.⁴³ For cysteine, because it is known from diffraction data that the molecule forms zwitterion structure, we took the zwitterion structure in the isolated state in a high dielectric constant (of water) environment as input structure to calculate the transition dipole directions. Each conformation is obtained by rotating the molecule along different single bonds. The bond lengths are relaxed during calculations. For determining the dihedral angle for the SH group, we fixed the positions of all heavy atoms and allowed only the SH group to rotate.

3. RESULTS AND DISCUSSION

3.1. Molecular Conformations of Orthorhombic L-Cysteine. L-cysteine has two major crystal forms, an orthorhombic phase (L-cysteine-I) and a monoclinic phase (L-cysteine-II).^{36–38} L-Cysteine molecules in both phases adopt

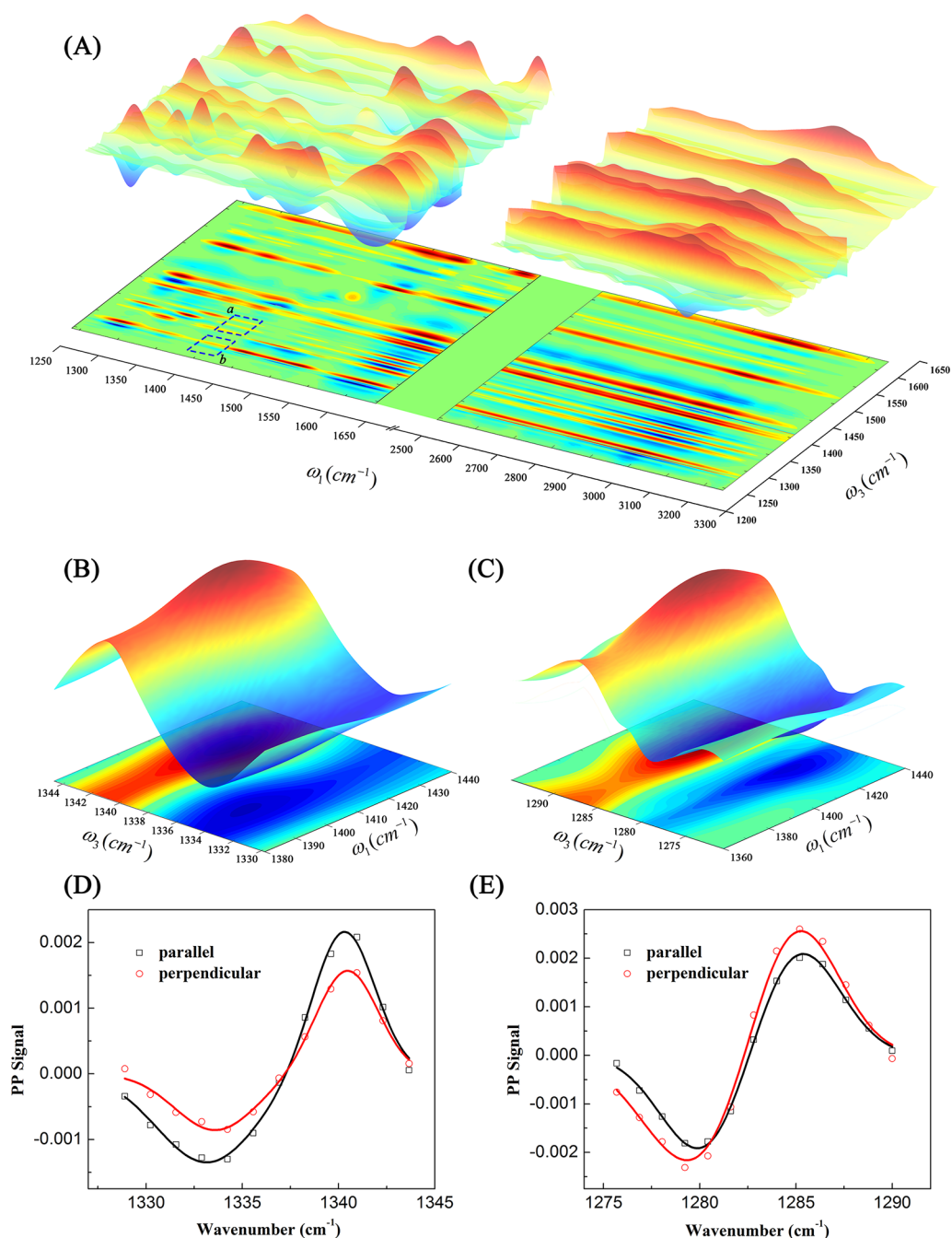


Figure 3. (A) Multiple-mode 2D-IR spectrum of the L-cysteine sample at waiting time 0.2 ps with the polarization of the detection beam perpendicular to that of the excitation beam. The relative intensities of peaks are adjusted to be comparably visible by multiplying the raw data with constants, which are listed in the Supporting Information. (B) Enlarged 2D-IR spectrum for the cross peak pair of δ CH₂ (ω_1) and δ CH (ω_3) (region a in panel A), and (C) enlarged 2D-IR spectrum for the cross peak pair between δ CH₂ (ω_1) and δ CH and ν_s COO⁻ (ω_3) frequency range (region b in panel A). (D) A slice cut along $\omega_1 = 1424$ cm⁻¹ of panel B with the polarization of the excitation both parallel (||) and perpendicular (⊥) to the polarization of the detection beam and (E) a slice cut along $\omega_1 = 1424$ cm⁻¹ of panel C with the polarization of the excitation both parallel (||) and perpendicular (⊥) to the polarization of the detection beam. The solid lines denote Gaussian peak fits. Because the vibrational cross angles are different, the relative intensities of the parallel and perpendicular signals are very different in D and E.

the zwitterion structure, and the molecular conformations of L-cysteine in the crystals have been thoroughly characterized through various methods.^{36–38} The sample in this study is mainly composed of the orthorhombic form, based on the XRD measurements (data are provided in the Supporting Information). A molecular conformation of L-cysteine in this crystal is illustrated in Figure 2A. The L-cysteine molecule has four major single bonds (S(1)–C(2), C(2)–C(3), C(3)–C(4), and

C(3)–N(5)). The rotations about these four bonds can generate many different conformations defined by the four dihedral angles: α (\angle S(1)C(2)/C(3)N(5)), β (\angle N(5)C(3)/C(4)O(7)), γ (\angle C(4)C(3)/N(5)H(13)), or γ' (\angle C(2)C(3)/N(5)H(14)), δ (\angle H(8)S(1)/C(2)C(3)). According to diffraction measurements,³⁶ the orthorhombic L-cysteine has two conformations. Both conformations have the same dihedral angles $\beta = -17^\circ$ and $\gamma = 64^\circ$. The α values are slightly different:

$\alpha_A = 60^\circ$ and $\alpha_B = 69^\circ$, and the δ values are very different: $\delta_A = 78^\circ$ and $\delta_B = -85^\circ$. The different δ values are caused by the torsion of SH group to form different H-bonds. The population ratio of these two conformations was estimated to be 1/1 from the diffraction measurements.

3.2. Vibrational Cross Angle Measurements. To determine the conformations of L-cysteine in the crystal, we followed the general procedure described in our previous work.^{30,32,34} (1) experimentally measure the cross angles of many vibrational modes that are sensitive to the changes of the dihedral angles, and (2) convert these vibrational cross angles into chemical bond dihedral angles with the aid of ab initio calculations. Figure 2A illustrates the basic concept of measuring the cross angle between two different vibrational modes. A linearly polarized IR pulse excites a vibrational mode, e.g., the NH_3 bending. After a very short period of time (0.1–0.2 ps, different from a typical all-fs setup,²³ we rarely see coherent artifacts that do not follow the anisotropy determined by the excitation and detection modes at \sim time zero for our fs/ps setup. For example, at time ~ 0 , we see the initial anisotropy value close to 0.4 for the OD stretch in D_2O , 0.4 for the CN stretch in the KSCN solutions.^{26,42} The rotational dynamics of both species are identical to those measured with the all-fs setups.^{44,45}) before the molecular rotation or conformational changes or intermolecular energy exchange have occurred for a substantial extent, another linearly polarized pulse of different frequencies detects a signal generated from the response of another vibrational mode, e.g. CH_2 bending, to the excitation of the NH_3 bending. In general, the excitation of one vibrational mode can lead to the vibrational frequency shift of another mode because of the anharmonic coupling.⁴⁶ The coupling produces a cross peak pair in the experimental 2D spectrum similar to those in Figure 3B,C. In addition to the vibrational coupling, the thermal effects induced by the relaxation of vibrational excitation and the direct vibrational energy transfer between the excited and detected modes can also produce cross peaks, which can have similar or different frequencies from those of cross peaks because of vibrational coupling in the 2D IR spectrum.³⁰ At very short waiting times before any rotational or conformational motion or intermolecular energy dissipation has occurred for a substantial amount,³³ the signals from all the three contributions are waiting-time dependent, the amplitudes of these cross peaks are dependent on the polarizations of the exciting and detecting beams, and the cross angle θ between the transition dipole moment directions of the excited and detected modes. For a sample isotropically distributed within the laser focus spot, the vibrational cross angle θ can be straightforwardly determined based on the equation^{32,47}

$$\frac{I_{\perp}}{I_{\parallel}} = \frac{2 - \cos^2 \theta}{1 + 2 \cos^2 \theta} \quad (1)$$

where I_{\parallel} , I_{\perp} are cross peak intensities with parallel and perpendicular excitation/detection polarizations as illustrated in Figure 3D,E, respectively. θ is the transition dipole moment cross angle between two coupled modes.

Experimentally, the vibrational cross angle is determined in the range between 0° and 90° . For a molecule rotating about a bond from 0° to 360° , a measured vibrational cross angle typically corresponds to more than one chemical bond dihedral angles (an example is provided in Figure S4 in the Supporting Information). Therefore, in order to obtain a single value for a

dihedral angle, more than one vibrational cross angles are required. In general, more vibrational cross angles give more precise results, not only because of the reason mentioned above, but also because more measurements can reduce random noise. Based on the reasoning, we scanned the 2D IR spectrum of the L-cysteine sample from $\sim 1250 \text{ cm}^{-1}$ to $\sim 3250 \text{ cm}^{-1}$. The spectrum from the perpendicular polarization configuration is shown in Figure 3A. Figure 3B,C shows enlarged spectra of the cross peak pairs between mode $\delta \text{ CH}_2$ and mode $\delta \text{ CH}$, and between mode $\delta \text{ CH}_2$ and mode $\delta \text{ CH}$ and $\nu_s \text{ COO}^-$, respectively. The peak assignments are based on the literature^{48,49} and DFT calculations. In Figure 3B, the excitation frequency $\omega_1 = 1424 \text{ cm}^{-1}$ is the CH_2 bending 0–1 transition frequency, indicating that the cross peak pair is from the CH_2 bending excitation. The detection frequency (red peak) $\omega_3 = 1341 \text{ cm}^{-1}$ is the CH bending 0–1 transition frequency, indicating that the cross peak pair is from the 0–1 transition frequency shift of the CH bending from 1341 cm^{-1} (red peak) to 1333 cm^{-1} (blue peak) caused by the CH_2 excitation. Figure 3D is a slice cut along $\omega_1 = 1424 \text{ cm}^{-1}$ of Figure 3B with the polarization of the excitation both parallel (\parallel) and perpendicular (\perp) to the polarization of the detection beam. The intensity peak ratio (I_{\perp}/I_{\parallel}) is ~ 0.58 . Based on eq 1 and this ratio, the vibrational cross angle is determined to be $\sim 36^\circ$ between the two vibrational modes: $\delta \text{ CH}_2$ (ω_1) and $\delta \text{ CH}$ (ω_3). The peak intensity ratio in Figure 3E is ~ 1.4 , which gives a vibrational cross angle of $\sim 67^\circ$ between the other pair of modes. Following the same procedure, we determined eight vibrational cross angles among eight pairs of vibrational modes to derive the different dihedral angles of the L-cysteine molecule in the sample. The measured cross angles are listed in Table 1.

Table 1. Vibrational Cross Angles between Coupled Vibrational Modes of the L-Cysteine, All of Which Are Determined from the Anisotropy Measurements

pair number	coupled modes	relative angle (degree)
1	$\delta_s \text{ NH}_3^+ / \delta_a \text{ NH}_3^+$	32
2	$\delta \text{ CH}_2 / \delta_a \text{ NH}_3^+$	73
3	$\nu \text{ CC}$ and $\delta \text{ CH} / \delta_s \text{ NH}_3^+$	60
4	$\delta \text{ CH}$ and $\nu_s \text{ COO}^- / \delta_a \text{ NH}_3^+$	43
5	$\delta_s \text{ NH}_3^+ / \delta \text{ CH}_2$	53
6	$\nu \text{ CC}$ and $\delta \text{ CH} / \delta_s \text{ NH}_3^+$	62
7	$\delta \text{ CH}_2 / \delta \text{ CH}$ and $\nu_s \text{ COO}^-$	67
8	$\delta \text{ CH}_2 / \delta \text{ CH}$	36

The experimental data are provided in the Supporting Information. The cross peaks involving the NH_3 stretch, the CH stretch, and the SH stretch were not used in the analysis, because we found that the NH_3 stretch peaks are extremely broad (Figure 2B and Figure 3A), and they severely overlap with the CH stretch and the SH stretch. The frequency overlaps impose great difficulties in properly deriving the vibrational cross angle for each pair of vibrations associated with these modes.

3.3. Convert Cross Angles into Dihedral Angles. As described in previous works,^{27,30,32,34} the measured vibrational cross angles can be converted into chemical bond dihedral angles with the aid of ab initio calculations, despite the fact that the vector direction of the transition dipole moment of a vibrational mode is typically different from the direction of the chemical bond that is mainly responsible for the vibration. The general procedure is to preset all possible molecular

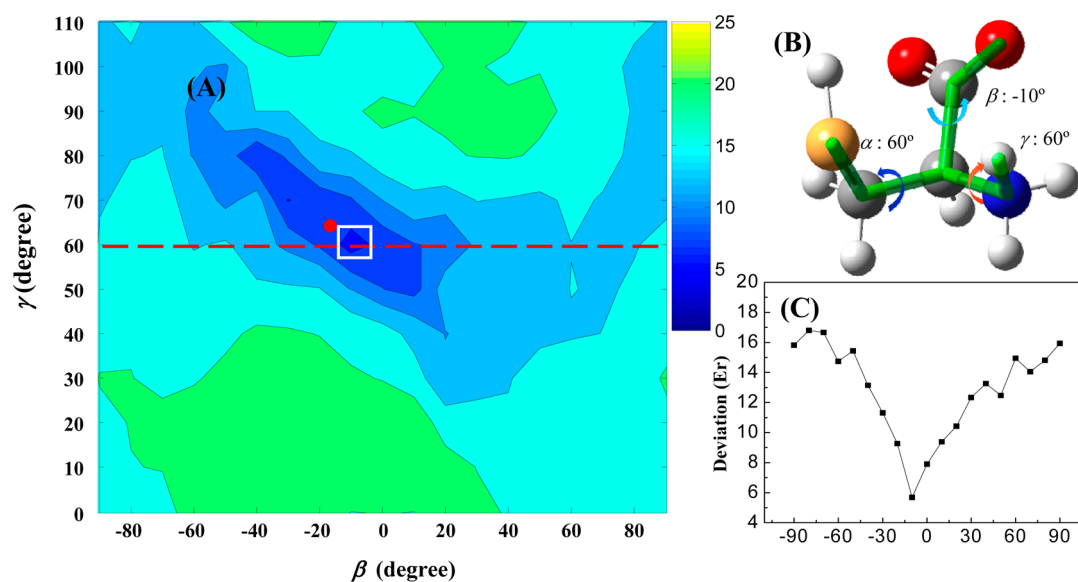


Figure 4. (A) The average difference Er between the experimental and calculated vibrational cross angles of the sample with different dihedral angles β and γ and fixed dihedral angle $\alpha = 60^\circ$. The z-axis is the amplitude of Er . The minimum Er value is labeled with white box. The red dot indicates angles determined by neutron diffraction. (B) The derived most probable molecular conformation in the sample. (C) A slice cut along $\gamma = 60^\circ$ of panel A.

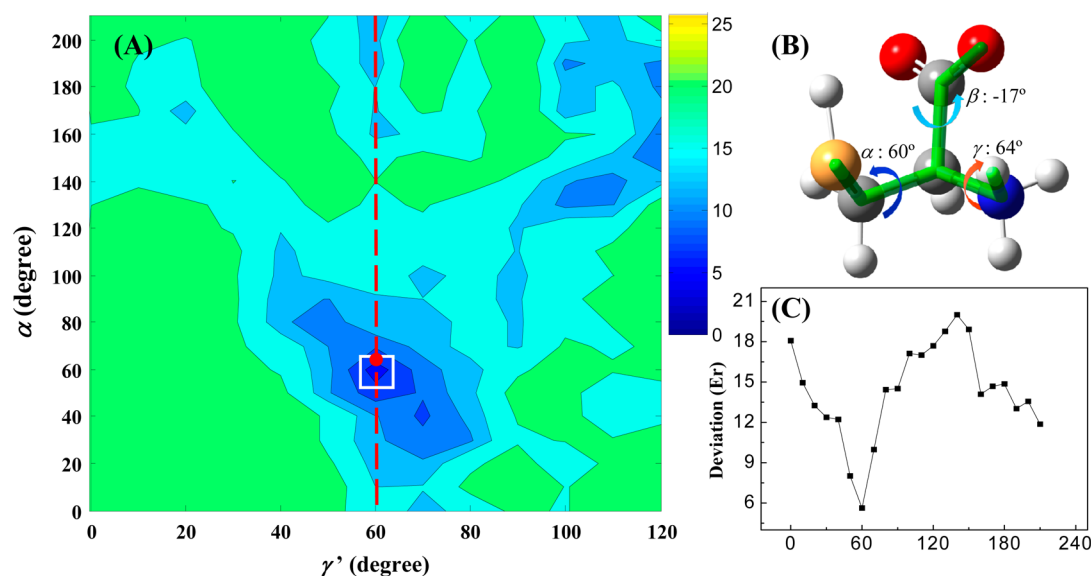


Figure 5. (A) The average difference Er between the experimental and calculated vibrational cross angles of the sample with different dihedral angles α and γ' and a fixed dihedral angle $\beta = -17^\circ$. The z-axis is the amplitude of Er . The minimum Er value is labeled with a white box. The red dot indicates the average angles determined by neutron diffraction. (B) The derived most probable molecular conformation in the sample. (C) A slice cut along $\gamma' = 60^\circ$ ($\gamma = 64^\circ$) of panel A.

conformations by rotating the molecules about all internal rotational degrees of freedom with the rotational step of several degrees, which we typically set to be 10° , and then calculate the vibrational cross angles of these preset conformations. The calculated vibrational cross angles of each conformation are compared to those experimentally measured. The preset conformation(s) which has (have) calculated vibrational cross angles closest to the experimental values is (are) considered as the most probable conformation(s) determined by the method. The similarity between the calculated and experimental cross angles is defined by the average deviation Er :

$$Er = \frac{\sum_{i=1}^m |A_i^C - A_i^E|}{m} \quad (2)$$

where A_i^C are the calculated vibrational cross angles of i th pair of normal modes for a specific conformation. A_i^E are the experimental values listed in Table 1. m is the number of the coupling pairs ($m = 8$ in this work). We consider the conformation giving the minimum Er is the most probable conformation determined by the method.

3.3.1. Determining Dihedral Angles β and γ . As discussed above, L-cysteine has four major single bonds. The rotations about these bonds for every 10° can produce enormous amounts of conformations that are too many to be practically

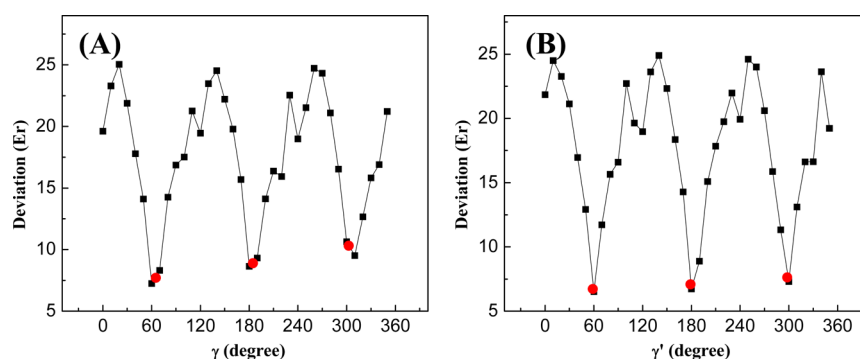


Figure 6. The average difference E_r between the experimental and calculated vibrational cross angles of the sample with fixed dihedral angles $\alpha = 65^\circ$, $\beta = -17^\circ$ and different dihedral angle (A) γ and (B) γ' . The red dots indicate angles determined by neutron diffraction.

calculated with high level ab initio calculations. To alleviate the difficulty, we used some molecular knowledge about the sample to reduce the calculation load. First of all, according to the literature,⁵⁰ the dihedral angle α is relatively rigid. It usually adopts values around 60° (the gauche⁺ conformer), -60° (the gauche⁻ conformer) and 180° (trans) for a typical amino acid. The other dihedral angles β , γ , and δ are more flexible, and usually determined by intermolecular interactions, e.g., the formation of N–H...O hydrogen bonds, S–H...O, or S–H...S hydrogen bonds. In L-cysteine-I at ambient condition, only the gauche⁺ conformation exists,³⁶ similar to the observation that most residues in peptides are in well-defined conformations with a strong preference for the gauche⁺ conformation.⁵⁰ Therefore, we can start calculations with a fixed dihedral angle $\alpha = 60^\circ$ to find other different dihedral angles. After the other angles are found, we can then come back to search for the optimal value for α . Second, the vibrational modes associated with the vibrational cross angles used in the analysis do not contain any significant contribution from the S atom. We can therefore assume that the value of dihedral angle δ does not affect these vibrational cross angles as much as the other three dihedral angles in the initial calculation and consider it as a free parameter determined by the calculation based on the energy minimum criterion. Third, because of the symmetry of NH_3^+ group and that of COO^- group, the ranges of β and γ are smaller than 360° . Based on the above considerations, in the initial calculation to map the bond dihedral angles, we varied the dihedral angle β from -90° to 90° and γ from 0° to 110° for every 10° , with a fixed $\alpha = 60^\circ$ and a free δ . The calculated vibrational cross angles from each of the conformations defined by these dihedral angles are compared to the experimental results, and the average deviation E_r defined in eq 2 from the comparison is plotted in Figure 4A. A global minimum of E_r is clearly found at the dihedral angles: $\beta = -10^\circ$ and $\gamma = 60^\circ$, which is labeled with a white box in Figure 4A. A slice cut along $\gamma = 60^\circ$ of Figure 4A is plotted in Figure 4C. The minimum of E_r can clearly be seen at $\beta = -10^\circ$. The molecular conformation defined by these angles is depicted in Figure 4B. The two dihedral angles ($\beta = -10^\circ$ and $\gamma = 60^\circ$) determined from the vibrational transition moment cross angle method are very close to those ($\beta = -17^\circ$ and $\gamma = 64^\circ$) determined by the neutron diffraction method, which is at the location of the red dot in Figure 4A.³⁶ Within experimental uncertainty, which is estimated to be $\sim 10^\circ$, we consider the two results as identical.

3.3.2. Determining Dihedral Angles α and γ' . We then come back to search for the dihedral angle α by setting $\beta =$

-17° and varying dihedral angle γ' (there is a one-to-one correspondence between γ' and γ) from 0° to 120° and α from 0° to 210° for every 10° . The average difference E_r versus the two dihedral angles from the mapping is plotted in Figure 5A. A global minimum of E_r is found at the dihedral angles: $\alpha = 60^\circ$ and $\gamma' = 60^\circ$, which corresponds to $\gamma = 64^\circ$. The minimum is labeled with a white box in Figure 5A. The optimal value of α can also be easily found from a slice cut along $\gamma' = 60^\circ$ (Figure 5C). The corresponding conformation is depicted in Figure 5B. Again, the determined dihedral angles are very close to those ($\alpha = 65^\circ$ (average of 60° and 69°), $\gamma = 64^\circ$) determined by neutron diffraction,³⁶ the location of which is marked as red dot in Figure 5A. Setting $\beta = -10^\circ$ and $\gamma = 60^\circ$ (results from 3.3.1) to map the optimal value for α also gives $\alpha = 60^\circ$ (Figure S4 in the Supporting Information). The result confirms that the L-cysteine molecule in the sample adopts the gauche⁺ conformation ($\alpha = 60^\circ$), verifying the validity of choosing $\alpha = 60^\circ$ as the initial input parameters to search for other dihedral angles. The result also shows that the sample is not L-cysteine-II, because about 50% of L-cysteine-II exists as the trans conformation ($\alpha = 180^\circ$).³⁷

3.3.3. Determine the Relative Positions of H Atoms of NH_3^+ . As discussed above, different from the XRD method, the dihedral angles involving H atoms can be determined by the vibrational cross angle method relatively easily. To demonstrate this point, we use the H atoms of NH_3^+ as an example. Figure 6(A) displays the average difference E_r with the dihedral angle γ varying from 0° to 350° (the H positions are rotating), with α and β respectively fixed at 65° (the averaged value) and -17° , which are determined by the diffraction methods. It can be clearly seen that by changing the H position (the γ value), E_r changes substantially. The minimum E_r values can be found at $\gamma = 60^\circ$, 180° , and 310° . The result is very close to that determined by the neutron diffraction: $\gamma = 64^\circ$, 183° , and 302° . Varying the dihedral angle γ' give a similar outcome (Figure 6B).

The results imply an immediate application of the vibrational cross angle method as an accessory tool for the XRD method to help resolve the relative positions of H atoms, which in many cases are difficult to be resolved by XRD but important because they are involved in the H-bonds and other intermolecular interactions.

3.3.4. Determining the Dihedral Angles δ . Cysteine has unique ability to form a disulfide bond, which plays important roles in certain biological processes.^{51,52} However, the orientation of the thiol group (SH) in many cases is difficult to be accurately determined by XRD because it typically rotates

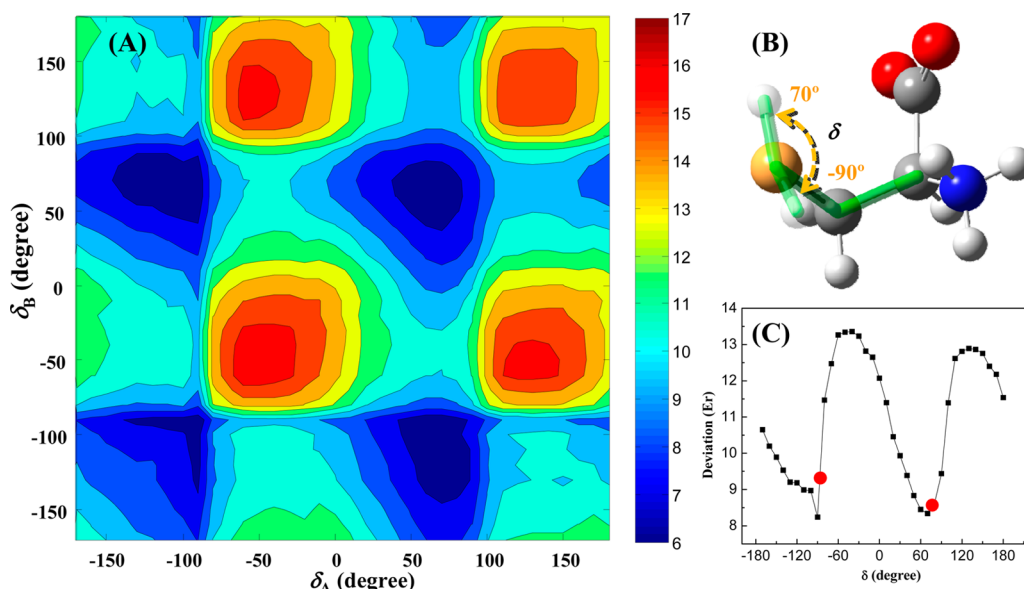


Figure 7. (A) The average difference E_r between the experimental and calculated average vibrational cross angles of the sample for mixtures with two different δ dihedral angles and fixed dihedral angles $\alpha = 65^\circ$, $\beta = -17^\circ$, and $\gamma = 64^\circ$. The z-axis is the amplitude of E_r . (B) Two derived most probable molecular conformations in the sample. (C) The averaged deviation E_r along any one of two axes in panel A versus the other axis. The red dots indicate angles determined by neutron diffraction.

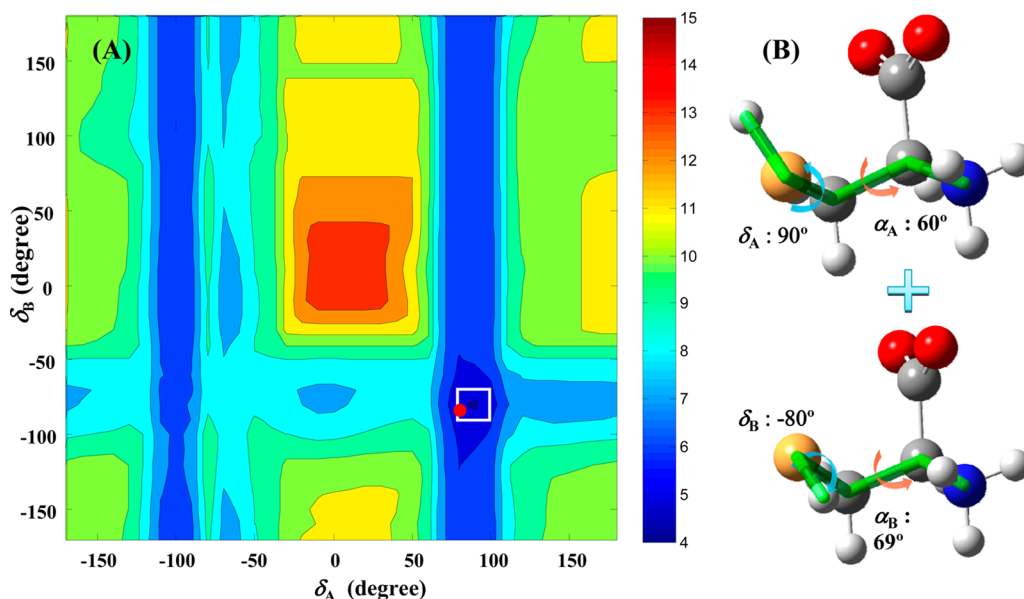


Figure 8. The average difference E_r between the experimental and calculated vibrational cross angles of the sample for different mixtures of two δ dihedral angles, which belong to two different conformations (conformation A and B). The z-axis is the amplitude of E_r . The red dot indicates angles determined by neutron diffraction with the disordered model. The global minimum of the deviation labeled with a white box corresponds to the dihedral angle of 90° for conformation A and -80° for conformation B, as depicted in the right panels.

very fast at room temperature. According to the disordered model,³⁶ two preferred orientations of SH (denoted as conformations A and B) coexist in the L-cysteine-I crystal with almost the same probability, leading to the formation of S–H...O and S–H...S hydrogen bonds, respectively. The corresponding dihedral angles δ are suggested to be $\delta_A = 78^\circ$ and $\delta_B = -85^\circ$, and the corresponding dihedral angles α are $\alpha_A = 60^\circ$ and $\alpha_B = 69^\circ$.

These two values of δ can also be determined by the vibrational cross angle method. For this mixture case, the calculated vibrational cross angles A_i^C in eq 2 must be replaced with the weighted combination of two possible cross angles. In

a system containing different sets of molecules, according to the additivity law of anisotropy, the total anisotropy is the weighted sum of the individual anisotropies:^{33,53}

$$R(t) = \sum_i f_i R_i(t) \quad (3)$$

where $R_i(t)$ is the anisotropy of each set and f_i is the signal fraction of each set. The average vibrational cross angle θ is related to the total anisotropy by

$$R = \frac{3 \cos^2 \theta - 1}{5} \quad (4)$$

Based on eqs 2, 3, and 4, the deviations Er for a mixture of two or more conformations can be calculated. Here one issue needs to be emphasized. f_i in eq 3 is the signal fraction. It is not necessarily the same as the molecular fraction of each set of conformation. As mentioned in our previous work,³³ these two quantities are identical only when the coupling responses are the same in different conformations. This condition is probably fulfilled for the current situation because the excitation and detection modes in the two conformations are respectively identical. We assume that the torsion angle of the SH group does not change the coupling response that much because the vibrational modes measured have relatively small contributions from the thiol group. Therefore, in calculating Er by varying δ_A and δ_B (Figure 7A), we took $f_i = 0.5$ (the same as the molar ratio), $\alpha = 65^\circ$ (the averaged value of two conformations), $\beta = -17^\circ$ and $\gamma = 64^\circ$. Four Er global minima reside in the locations of $\delta_A, \delta_B = -90^\circ, 70^\circ$. Because one conformation can have either δ_A or δ_B , the results indicate that δ can only be either -90° or 70° . The dependence of the average deviation for each conformation on the dihedral angle δ is plotted in Figure 7C. Two minima with $\delta = -90^\circ$ and 70° are clearly visible. They are very close to the neutron diffraction results marked as red dots in Figure 7C. The corresponding conformations are depicted in Figure 7B.

The above procedure is based on the preset percentage (50%) for each conformation. Here we use one strategy to test the reliability of the preset percentage. In the calculations for the vibrational cross angles of each conformation by varying δ_A and δ_B , we fixed all the coordinates of atoms as those determined from neutron diffraction method except the H atom in thiol group, and corresponding dihedral angles are $\delta = -17^\circ$, $\gamma = 64^\circ$, $\alpha_A = 60^\circ$, and $\alpha_B = 69^\circ$. In the calculations to obtain the average difference Er between calculated and experimental cross angles, we left f_i in eq 3 as a free parameter so that Er is a function of f_i . For each complete set of dihedral angles $\delta_A = x$, $\delta_B = y$, $\beta = -17^\circ$, $\gamma = 64^\circ$, $\alpha_A = 60^\circ$, and $\alpha_B = 69^\circ$ (x, y are arbitrary numbers between -180° to 180°), there is a corresponding minimum Er by varying f_i . These minimum Er values versus δ_A and δ_B are plotted in Figure 8A. The smallest Er value in Figure 8A is located at $\delta_A = 90^\circ$, $\delta_B = -80^\circ$, labeled with a white box. f_i corresponding to this Er is 49% of conformation A (Figure 8B). Both dihedral angles $\delta_A = 90^\circ$, $\delta_B = -80^\circ$ are close to those (red dot in Figure 8A) from the neutron diffraction measurements: $\delta_A = 78^\circ$ and $\delta_B = -85^\circ$. $f_i = 49\%$ is also close to the estimation that conformations A and B are almost equally populated from the neutron diffraction measurements.

In summary, the conformations in the L-cysteine-I sample determined by the vibrational cross angle measurements are 49% of conformation A with $\delta_A = 80^\circ \pm 10^\circ$, $\beta = -10^\circ \pm 10^\circ$, $\gamma = 60^\circ \pm 10^\circ$, $\alpha_A = 60^\circ \pm 10^\circ$, and 51% of conformation B with $\delta_B = -80^\circ \pm 10^\circ$, $\beta = -10^\circ \pm 10^\circ$, $\gamma = 60^\circ \pm 10^\circ$, $\alpha_B = 60^\circ \pm 10^\circ$.

3.4. Difficulties and Perspective. The results described above demonstrate that the vibrational cross angle method has the potential to resolve conformations of relatively complex molecules with the aid of some prior known molecular knowledge. At the same time, this work raises many problems about this method that were not met in our previous studies, as the L-cysteine sample studied in this work is different from previous systems investigated with the same method.^{32–34} First of all, L-cysteine has four internal rotational degrees of freedom from which the calculation load is difficult to be dealt with by

ordinary personal computers equipped in a typical experimental lab. To save the computing time, the strategy used in this work to map all these four degrees of freedom is not a thorough searching scheme for the global minima. It is more like the approach to guess a range that the global minima should be based on some molecular knowledge and then search the minima in this range. There is always a risk that the initial guess can actually be a local minimum rather than a global one. A more statistically rigorous searching scheme that can balance between computational time and accuracy is needed in the future for resolving conformations of more complex molecules.

Second, there can be more than two conformations each of which is substantially populated in one sample. If these different conformations have distinct frequencies for some vibrational modes within the excitation or detection frequency range, the vibrational cross angles associated with these modes can be used to resolve each individual conformation as demonstrated in our previous work.³³ In the L-cysteine sample, there are no obvious frequency differences among the vibrational modes at frequencies above 1200 cm^{-1} in the two conformations. If we did not know that there are two conformations in the sample, we would only obtain a single $\delta = 80^\circ$ value (Figure S5 in the Supporting Information) rather than two. This single value is not the simple average of several values because the correlation between a bond dihedral angle and a vibrational cross angle is not a straightforward function. The difficulty can be alleviated by extending the detection down to far IR and T-Hz where more conformation-related vibrational modes of which the frequencies are sensitive to the chemical bond dihedral angles reside. This should be technically feasible as demonstrated in Figure 1 in which the far IR and T-Hz spectrum for the super continuum is successfully detected with a PMT. Our next step is to assemble the detection scheme into the 2D IR system.

Third, the vibrational peak assignment is another problem. For many vibrational modes with frequencies below 1700 cm^{-1} , their assignments are difficult because of at least two major reasons: (1) Fermi resonances among normal modes and combination bands or overtones, which generate new peaks that are difficult to be theoretically predicted; and (2) the calculated frequencies even with very high level calculations still have some noticeable uncertainties. Our general procedure to address this problem is to use the vibrational cross angles to help the assignments: find a few vibrational modes of which the assignments are well-defined, and then measure and calculate the vibrational cross angles between these modes and those unassigned modes. The comparison between calculated and measured cross angles is generally very helpful in telling the origins of the unknown peaks for relatively simple molecules if the candidate origins have very different transition dipole moment directions. One of our future plans to improve this approach is to accumulate the database for each type of molecules to build a set of empirical criteria to assign peaks.

Fourth, the frequency overlap among different modes is also a very severe problem. Experimentally we measured many more than the eight vibrational cross angles used in the analysis, but most of them were not used either because the peak assignments are not clear or the frequency overlap is too severe. In principle, this problem can be solved if the compositions of a peak and the signal contributions of different modes to it are known. In practice, it is relatively easy to obtain the compositions from calculations, but it is very difficult to know about the detailed contribution of each mode to the total signal of the peak because the vibrational couplings can not be

predicted very precisely by calculations.³⁴ At the current stage, it is probably more reliable to obtain the coupling strength between any two modes by experiments rather than by calculations. Again, a key step to alleviate the frequency overlap problem is to accumulate a database to understand how two vibrational modes are coupled and how the coupling affects the signal size.

The four issues discussed above are the major challenges we encounter in developing the vibrational cross angle method into a general molecular structural tool. They are practically very difficult but are not principally impossible. Here only a few very superficial ideas are proposed to address them. We believe that many better approaches will be developed with the progress of research in the future.

4. CONCLUDING REMARKS

In this work, the molecular conformations of crystalline L-cysteine prepared in its orthorhombic form were determined by the vibrational cross angle measurements. Its major dihedral angles of chemical bonds determined by this method are consistent with the results from diffraction experiments. In addition, we also demonstrate that the relative orientations of the chemical bonds associated with the hydrogen atoms of the NH₃⁺ group and the thiol group can also be determined by the method. The results demonstrate that the vibrational cross angle method based on the multiple-mode approach can potentially become a structural tool for determining molecular conformations, although we are still facing many challenges.

■ ASSOCIATED CONTENT

Supporting Information

Supporting figures and data about XRD measurements, 2D-IR measurements, anisotropy measurements, and data analyses. This material is available free of charge via the Internet at <http://pubs.acs.org>.

■ AUTHOR INFORMATION

Corresponding Author

*Tel: 001-713-348-2048. E-mail: junrong@rice.edu.

Notes

The authors declare no competing financial interest.

■ ACKNOWLEDGMENTS

This material is based upon work supported by the Welch foundation under Award No. C-1752, and the Air Force Office of Scientific Research under AFOSR Award No. FA9550-11-1-0070. J.Z. also thanks the David and Lucile Packard Foundation for a Packard fellowship.

■ REFERENCES

- (1) Vangunsteren, W. F.; Berendsen, H. J. C. Computer-Simulation as a Tool for Tracing the Conformational Differences between Proteins in Solution and in the Crystalline State. *J. Mol. Biol.* **1984**, *176*, 559–564.
- (2) Skrynnikov, N. R.; Goto, N. K.; Yang, D. W.; Choy, W. Y.; Tolman, J. R.; Mueller, G. A.; Kay, L. E. Orienting domains in proteins using dipolar couplings measured by liquid-state NMR: Differences in solution and crystal forms of maltodextrin binding protein loaded with beta-cyclodextrin. *J. Mol. Biol.* **2000**, *295*, 1265–1273.
- (3) Weissenhorn, W.; Dessen, A.; Calder, L. J.; Harrison, S. C.; Skehel, J. J.; Wiley, D. C. Structural basis for membrane fusion by enveloped viruses. *Mol. Membr. Biol.* **1999**, *16*, 3–9.

- (4) Torii, K.; Iitaka, Y. Crystal Structure of L-Valine. *Acta Crystallogr., Sect. B: Struct. Crystallogr. Cryst. Chem.* **1970**, *B 26*, 1317.
- (5) Torii, K.; Iitaka, Y. Crystal Structure of L-Isoleucine. *Acta Crystallogr., Sect. B: Struct. Crystallogr. Cryst. Chem.* **1971**, *B 27*, 2237.
- (6) Simpson, H. J.; Marsh, R. E. Crystal Structure of L-Alanine. *Acta Crystallogr.* **1966**, *20*, 550–.
- (7) Derissen, J. L.; Endeman, H. J.; Peerdema, Af. Crystal and Molecular Structure of L-Aspartic Acid. *Acta Crystallogr., Sect. B: Struct. Crystallogr. Cryst. Chem.* **1968**, *B 24*, 1349.
- (8) Hirokawa, S. A New Modification of L-Glutamic Acid and Its Crystal Structure. *Acta Crystallogr.* **1955**, *8*, 637–641.
- (9) Cochran, W.; Penfold, B. R. The Crystal Structure of L-Glutamine. *Acta Crystallogr.* **1952**, *5*, 644–653.
- (10) Tarakeshwar, P.; Manogaran, S. Vibrational Frequencies of Cysteine and Serine Zwitterions - an Ab-Initio Assignment. *Spectrosc. Acta Pt. A-Molec. Biomolec. Spectr.* **1995**, *51*, 925–928.
- (11) Pawlukoic, A.; Leciejewicz, J.; Ramirez-Cuesta, A.; Nowicka-Scheibe, J. L-Cysteine: Neutron spectroscopy, Raman, IR and ab initio study. *Spectrosc. Acta, Part A: Mol. Biomol. Spectrosc.* **2005**, *61*, 2474–2481.
- (12) Ernst, R. R.; Bodenhausen, G.; Wokaun, A. *Nuclear Magnetic Resonance in One and Two Dimensions*; Oxford University Press: Oxford, 1987.
- (13) Bifulco, G.; Dambruoso, P.; Gomez-Paloma, L.; Riccio, R. Determination of relative configuration in organic compounds by NMR spectroscopy and computational methods. *Chem. Rev.* **2007**, *107*, 3744–3779.
- (14) Jonas, D. M. Two-Dimensional Femtosecond Spectroscopy. *Annu. Rev. Phys. Chem.* **2003**, *54*, 425–463.
- (15) Dlott, D. D. Ultrafast Chemical Exchange Seen with 2D Vibrational Echoes. *Science* **2005**, *309*, 1333–1334.
- (16) Khalil, M.; Demirdoven, N.; Tokmakoff, A. Coherent 2D IR Spectroscopy: Molecular Structure and Dynamics in Solution. *J. Phys. Chem. A.* **2003**, *107*, 5258–5279.
- (17) Bredenbeck, J.; Helbing, J.; Hamm, P. Labeling vibrations by light: Ultrafast transient 2D-IR spectroscopy tracks vibrational modes during photoinduced charge transfer. *J. Am. Chem. Soc.* **2004**, *126*, 990–991.
- (18) Shim, S. H.; Strasfeld, D. B.; Ling, Y. L.; Zanni, M. T. Automated 2D IR spectroscopy using a mid-IR pulse shaper and application of this technology to the human islet amyloid polypeptide. *Proc. Natl. Acad. Sci. U.S.A.* **2007**, *104*, 14197–14202.
- (19) Nee, M. J.; Baiz, C. R.; Anna, J. M.; McCanne, R.; Kubarych, K. J. Multilevel vibrational coherence transfer and wavepacket dynamics probed with multidimensional IR spectroscopy. *J. Chem. Phys.* **2008**, *129*, 11.
- (20) Naraharisetty, S. R. G.; Kasyanenko, V. M.; Rubtsov, I. V. Bond connectivity measured via relaxation-assisted two-dimensional infrared spectroscopy. *J. Chem. Phys.* **2008**, *128*, 7.
- (21) Maekawa, H.; Formaggio, F.; Toniolo, C.; Ge, N. H. Onset of 3(10)-helical secondary structure in Aib oligopeptides probed by coherent 2D IR spectroscopy. *J. Am. Chem. Soc.* **2008**, *130*, 6556–6566.
- (22) Cowan, M. L.; Bruner, B. D.; Huse, N.; Dwyer, J. R.; Chugh, B.; Nibbering, E. T. J.; Elsaesser, T.; Miller, R. J. D. Ultrafast memory loss and energy redistribution in the hydrogen bond network of liquid H₂O. *Nature* **2005**, *434*, 199–202.
- (23) Zheng, J.; Kwak, K.; Asbury, J. B.; Chen, X.; Piletic, I.; Fayer, M. D. Ultrafast Dynamics of Solute-Solvent Complexation Observed at Thermal Equilibrium in Real Time. *Science* **2005**, *309*, 1338–1343.
- (24) Zheng, J.; Kwac, K.; Xie, J.; Fayer, M. D. Ultrafast Carbon-Carbon Single Bond Rotational Isomerization in Room Temperature Solution. *Science* **2006**, *313*, 1951–1955.
- (25) Bredenbeck, J.; Ghosh, A.; Smits, M.; Bonn, M. Ultrafast two dimensional-infrared spectroscopy of a molecular monolayer. *J. Am. Chem. Soc.* **2008**, *130*, 2152–.
- (26) Bian, H. T.; Wen, X. W.; Li, J. B.; Chen, H. L.; Han, S. Z.; Sun, X. Q.; Song, J. A.; Zhuang, W.; Zheng, J. R. Ion clustering in aqueous

solutions probed with vibrational energy transfer. *Proc. Natl. Acad. Sci. U.S.A.* **2011**, *108*, 4737–4742.

(27) Chen, H. L.; Zhang, Y. F.; Li, J. B.; Liu, H. J.; Jiang, D. E.; Zheng, J. R. Vibrational Cross Angles in Condensed Molecules: A Structural Tool. *J. Phys. Chem. A* **2013**, DOI: 10.1021/jp406304c.

(28) Li, J. B.; Bian, H. T.; Chen, H. L.; Hoang, B.; Zheng, J. R. Ion Association in Aqueous Solutions Probed through Vibrational Energy Transfers among Cation, Anion and Water Molecules. *J. Phys. Chem. B* **2013**, *117*, 4274–4283.

(29) Li, J. B.; Bian, H. T.; Wen, X. W.; Chen, H. L.; Yuan, K. J.; Zheng, J. R. Probing Ion/Molecule Interactions in Aqueous Solutions with Vibrational Energy Transfer. *J. Phys. Chem. B* **2012**, *116*, 12284–12294.

(30) Chen, H. L.; Bian, H. T.; Li, J. B.; Wen, X. W.; Zheng, J. R. Ultrafast multiple-mode multiple-dimensional vibrational spectroscopy. *Int. Rev. Phys. Chem.* **2012**, *31*, 469–565.

(31) Bian, H. T.; Li, J. B.; ZHANG, Q.; Chen, H. L.; Zhuang, W.; Gao, Y. Q.; Zheng, J. R. Ion Segregation in Aqueous Solutions. *J. Phys. Chem. B* **2012**, *116*, 14426–14432.

(32) Bian, H. T.; Li, J. B.; Chen, H. L.; Yuan, K. J.; Wen, X. W.; Li, Y. Q.; Sun, Z. G.; Zheng, J. R. Molecular Conformations and Dynamics on Surfaces of Gold Nanoparticles Probed with Multiple-Mode Multiple-Dimensional Infrared Spectroscopy. *J. Phys. Chem. C* **2012**, *116*, 7913–7924.

(33) Chen, H. L.; Bian, H. T.; Li, J. B.; Wen, X. W.; Zheng, J. R. Relative Intermolecular Orientation Probed via Molecular Heat Transport. *J. Phys. Chem. A* **2013**, DOI: 10.1021/jp312604v.

(34) Bian, H. T.; Li, J. B.; Wen, X. W.; Sun, Z. G.; Song, J. A.; Zhuang, W.; Zheng, J. R. Mapping Molecular Conformations with Multiple-Mode Two-Dimensional Infrared Spectroscopy. *J. Phys. Chem. A* **2011**, *115*, 3357–3365.

(35) Bian, H. T.; Chen, H. L.; Li, J. B.; Wen, X. W.; Zheng, J. R. Nonresonant and resonant mode-specific intermolecular vibrational energy transfers in electrolyte aqueous solutions. *J. Phys. Chem. A* **2011**, *115*, 11657–11664.

(36) Kerr, K. A.; Ashmore, J. P.; Koetzle, T. F. Neutron-Diffraction Study of L-Cysteine. *Acta Crystallogr. Sect. B-Struct. Commun.* **1975**, *31*, 2022–2026.

(37) Harding, M. M.; Long, H. A. Crystal and Molecular Structure of L-Cysteine. *Acta Crystallogr., Sect. B: Struct. Crystallogr. Cryst. Chem.* **1968**, *B 24*, 1096.

(38) Gorbitz, C. H.; Dalhus, B. L-Cysteine, monoclinic form, redetermination at 120 K. *Acta Crystallogr., Sect. C: Cryst. Struct. Commun.* **1996**, *52*, 1756–1759.

(39) Dai, J.; Xie, X.; Zhang, X. C. Detection of broadband terahertz waves with a laser-induced plasma in gases. *Phys. Rev. Lett.* **2006**, *97*, 4.

(40) Petersen, P. B.; Tokmakoff, A. A source for ultrafast continuum infrared and terahertz radiation. *Opt. Lett.* **2010**, *35*, 1962–1964.

(41) Calabrese, C.; Stingel, A. M.; Shen, L.; Petersen, P. B. Ultrafast continuum mid-infrared spectroscopy: Probing the entire vibrational spectrum in a single laser shot with femtosecond time resolution. *Opt. Lett.* **2012**, *37*, 2265–2267.

(42) Bian, H. T.; Wen, X. W.; Li, J. B.; Zheng, J. R. Mode-specific intermolecular vibrational energy transfer. II. Deuterated water and potassium selenocyanate mixture. *J. Chem. Phys.* **2010**, *133*, 034505.

(43) Dong, F.; Miller, R. E. Vibrational transition moment angles in isolated biomolecules: A structural tool. *Science* **2002**, *298*, 1227–1230.

(44) Rezus, Y. L. A.; Bakker, H. J. On the orientational relaxation of HDO in liquid water. *J. Chem. Phys.* **2005**, *123*, 7.

(45) Lenchenkov, V.; She, C. X.; Lian, T. Q. Vibrational relaxation of CN stretch of pseudo-halide anions (OCN⁻, SCN⁻, and SeCN⁻) in polar solvents. *J. Phys. Chem. B* **2006**, *110*, 19990–19997.

(46) *Ultrafast Infrared and Raman Spectroscopy*; Fayer, M. D., Ed.; Marcel Dekker, Inc: New York/Basel, 2001; Vol. 26.

(47) Lawkowitz, J. *Principles of Fluorescence Spectroscopy*, 3rd ed.; Springer: New York, 2006.

(48) Susi, H.; Byler, D. M.; Gerasimowicz, W. V. Vibrational Analysis of Amino-Acids - Cysteine, Serine, Beta-Chloroalanine. *J. Mol. Struct.* **1983**, *102*, 63–79.

(49) Barth, A. The infrared absorption of amino acid side chains. *Prog. Biophys. Mol. Biol.* **2000**, *74*, 141–173.

(50) Gorbitz, C. H. Conformational Properties of the Amino-Acid-Residues L-Cysteine, L-Serine and L-Cystine. *Acta Chem. Scand.* **1990**, *44*, 584–590.

(51) Gregoret, L. M.; Rader, S. D.; Fletterick, R. J.; Cohen, F. E. Hydrogen-Bonds Involving Sulfur-Atoms in Proteins. *Proteins: Struct., Funct., Genet.* **1991**, *9*, 99–107.

(52) Zhou, P.; Tian, F. F.; Lv, F. L.; Shang, Z. C. Geometric characteristics of hydrogen bonds involving sulfur atoms in proteins. *Proteins* **2009**, *76*, 151–163.

(53) Valeur, B. *Molecular Fluorescence: Principles and Applications*; Wiley-VCH: Weinheim, Germany, 2002.

Supporting Information

Molecular Conformations of Crystalline L-Cysteine Determined with Vibrational Cross Angle Measurements

Hailong Chen, Hongtao Bian, Jiebo Li, Xunmin Guo, Xiewen Wen, Junrong Zheng*

Department of Chemistry, Rice University, Houston, TX 77005, USA

* To whom correspondence should be addressed. Tel: 001-713-348-2048. E-mail:

junrong@rice.edu

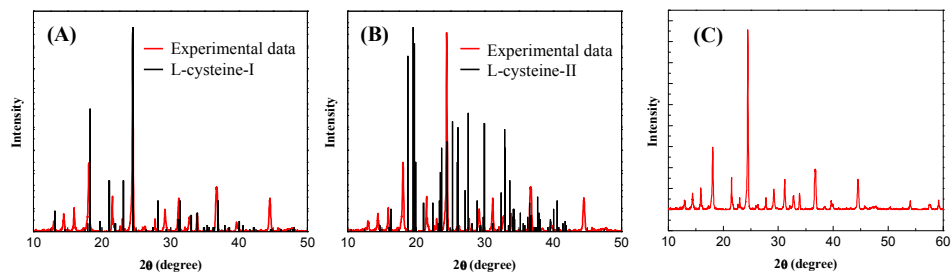


Figure S1. XRD spectrum (C) of the L-cysteine sample (the sample measured in 2D IR experiments), which is mainly consisted of the orthorhombic phase by comparing the spectrum with diffraction database of L-cysteine-I¹ (A) and L-cysteine-II² (B) respectively.

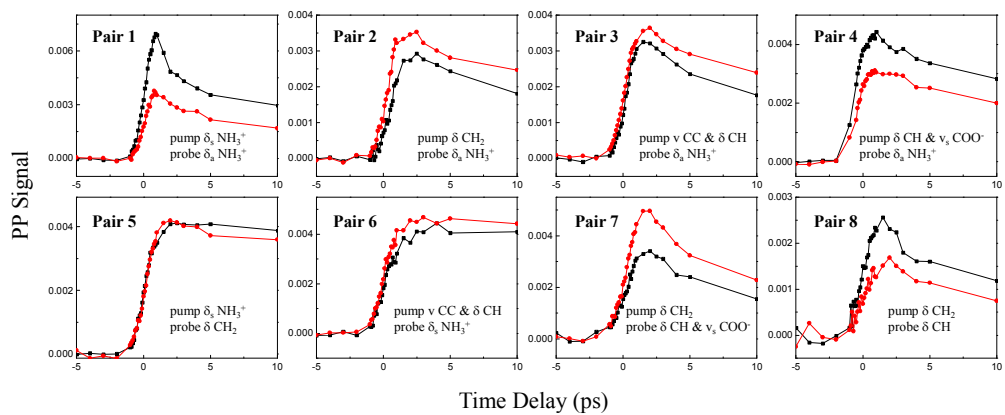


Figure S2. Polarization selective pump/probe data for all the measured pairs of coupled vibrational modes listed in table 1.

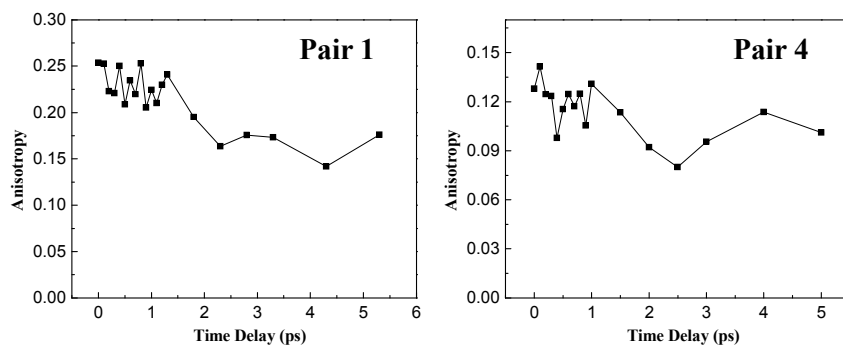


Figure S3. *Waiting time dependent anisotropy data of cross peak pairs 1&4, calculated based on the data shown in fig. S2. The anisotropic decay is slow within 1 ps after excitation, with the initial value almost unchanged. It indicates a relatively slow rotational relaxation rate of the molecule. After 1 ps, the anisotropy slightly decays. The slight anisotropy decay can be from two origins. One is the wobbling motions of the molecule, and the other is the intermolecular heat transport from vibrational relaxations. Estimated from the signal decays in fig.S2, the lifetimes of the vibrational modes are about 1~2 ps. It is conceivable that after 1-2 ps, the vibrational excitations have relaxed into low frequency vibrations and heat and dissipate to other molecules. Such heat dissipations are typically random and can change the anisotropy to a certain value which is determined by the detailed intermolecular orientations of the sample.³*

Table S1. *Scaling factors for the multiple-mode 2D IR spectrum shown in fig. 3A.*

Region	Dividing factor ($\times 10^{-5}$)	Region	Dividing factor ($\times 10^{-5}$)
Pump 1440-1640 cm^{-1} Probe 1244-1280 cm^{-1}	5.5	Pump 1440-1520 cm^{-1} Probe 1280-1320 cm^{-1}	3.8
Pump 1540-1640 cm^{-1} Probe 1280-1320 cm^{-1}	15.0	Pump 1440-1520 cm^{-1} Probe 1320-1364 cm^{-1}	1.2
Pump 1540-1640 cm^{-1} Probe 1320-1364 cm^{-1}	5.3	Pump 1440-1640 cm^{-1} Probe 1364-1410 cm^{-1}	9.7
Pump 1440-1640 cm^{-1} Probe 1410-1460 cm^{-1}	11.4	Pump 1440-1640 cm^{-1} Probe 1496-1555 cm^{-1}	15.9
Pump 1560-1640 cm^{-1} Probe 1555-1625 cm^{-1}	9.7		
Pump 1240-1440 cm^{-1} Probe 1244-1280 cm^{-1}	7.2	Pump 1240-1440 cm^{-1} Probe 1280-1320 cm^{-1}	11.5
Pump 1240-1440 cm^{-1} Probe 1320-1364 cm^{-1}	5.0	Pump 1240-1440 cm^{-1} Probe 1364-1410 cm^{-1}	4.0
Pump 1240-1440 cm^{-1} Probe 1410-1460 cm^{-1}	3.4	Pump 1240-1440 cm^{-1} Probe 1496-1555 cm^{-1}	5.7
Pump 1240-1540 cm^{-1} Probe 1555-1625 cm^{-1}	4.0		
Pump 2500-3250 cm^{-1} Probe 1244-1280 cm^{-1}	5.6	Pump 2500-3250 cm^{-1} Probe 1280-1320 cm^{-1}	17.1
Pump 2500-3250 cm^{-1} Probe 1320-1364 cm^{-1}	9.8	Pump 2500-3250 cm^{-1} Probe 1364-1410 cm^{-1}	9.0

Pump 2500-3250 cm^{-1} Probe 1410-1460 cm^{-1}	14.3	Pump 2500-3250 cm^{-1} Probe 1496-1555 cm^{-1}	38.3
Pump 2500-3250 cm^{-1} Probe 1555-1625 cm^{-1}	20.0		

Table S2. The assignment of major IR peaks in the whole spectrum range (in cm^{-1}) for the L-cysteine sample.

vibrational mode	IR Peak (cm^{-1})
νNH_3^+	broad peaks above 2000 cm^{-1}
$\nu_a \text{CH}_2$	2995
$\nu_s \text{CH}_2$ & νCH	2946
νSH	2543
$\delta_a \text{NH}_3^+$	1608
$\nu_s \text{COO}^-$	1581
$\delta_a \text{NH}_3^+$	1552
$\delta_s \text{NH}_3^+$	1511
δCH_2	1424
νCC & δCH	1396
δCH	1343
δCH & $\nu_s \text{COO}^-$	1290
$\rho^\perp \text{NH}_3^+$	1138

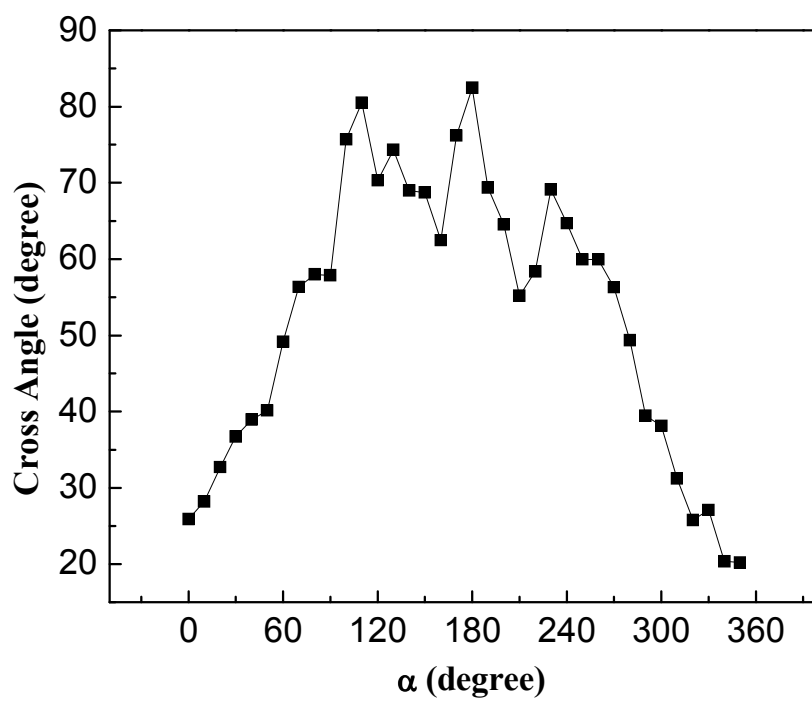


Figure S4. *The correlation between the dihedral angle α and the vibrational cross angle between $\delta NH_3^+ / \delta CH_2$ with fixed $\beta = -10^\circ$ and $\gamma = 60^\circ$.*

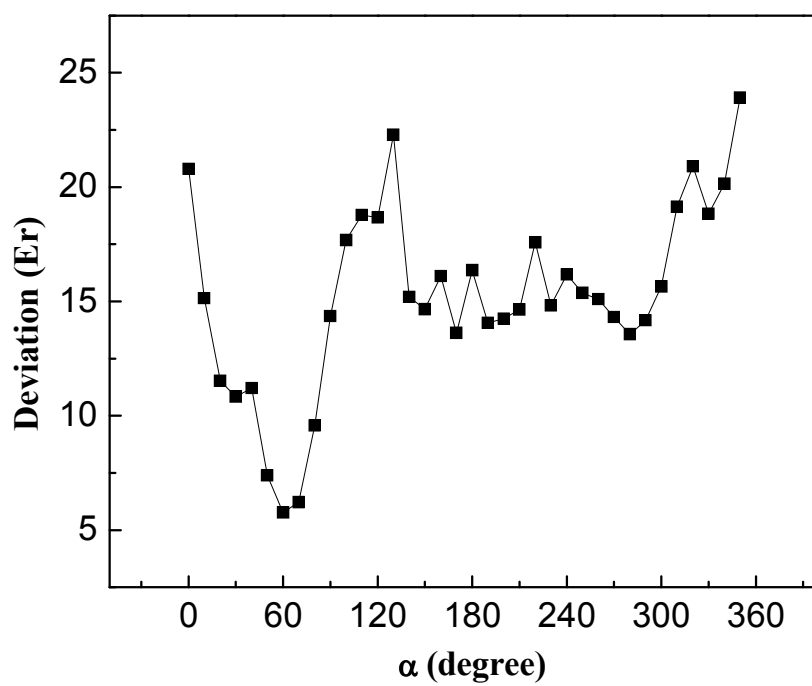


Figure S5. The average difference Er between calculated and experimental vibrational cross angles vs. α with fixed $\beta = -10^\circ$ and $\gamma = 60^\circ$.

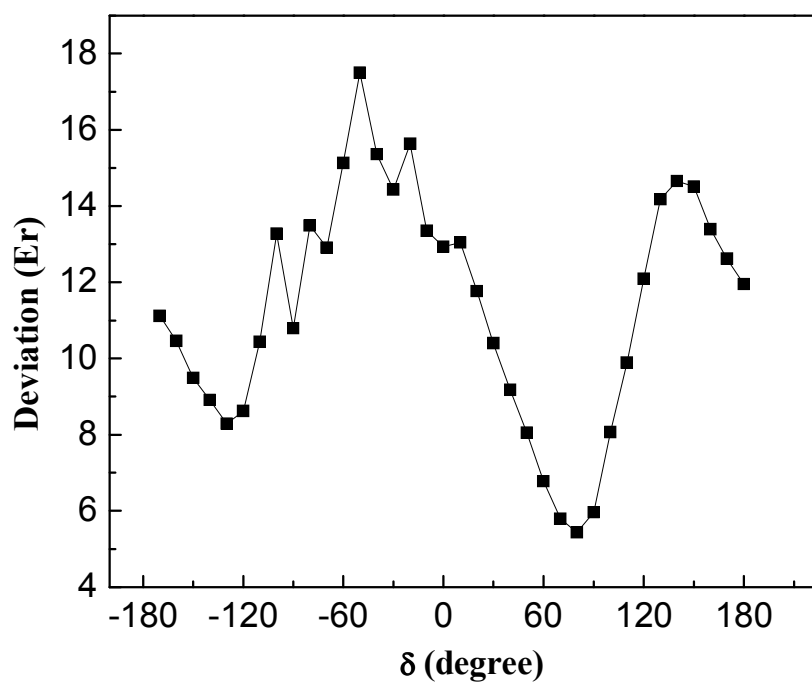


Figure S6. The average difference Er between calculated and experimental vibrational cross angles vs. δ with fixed $\alpha = 60^\circ$, $\beta = -10^\circ$ and $\gamma = 60^\circ$.

References

- (1) Powder Diffraction File, Card No. 00-032-1636, International Centre for Diffraction Data, Newtown Square, PA
- (2) Powder Diffraction File, Card No. 00-024-1928, International Centre for Diffraction Data, Newtown Square, PA
- (3) Chen, H. L.; Bian, H. T.; Li, J. B.; Wen, X. W.; Zheng, J. R. Relative intermolecular orientation probed via molecular heat transport. *J. Phys. Chem. A.* 2013, 117, pp.6052-6065.